

Lab on a Chip

Accepted Manuscript



This is an *Accepted Manuscript*, which has been through the Royal Society of Chemistry peer review process and has been accepted for publication.

Accepted Manuscripts are published online shortly after acceptance, before technical editing, formatting and proof reading. Using this free service, authors can make their results available to the community, in citable form, before we publish the edited article. We will replace this *Accepted Manuscript* with the edited and formatted *Advance Article* as soon as it is available.

You can find more information about *Accepted Manuscripts* in the [Information for Authors](#).

Please note that technical editing may introduce minor changes to the text and/or graphics, which may alter content. The journal's standard [Terms & Conditions](#) and the [Ethical guidelines](#) still apply. In no event shall the Royal Society of Chemistry be held responsible for any errors or omissions in this *Accepted Manuscript* or any consequences arising from the use of any information it contains.

Title

Multiplexed detection of viral infections using rapid *in-situ* RNA analysis on a chip

Authors

Sydney M. Shaffer^{1,2,*}, Rohan P. Joshi^{2,*}, Benjamin S. Chambers³, David Sterken², Andrew G. Biaisch¹, David J. Gabrieli¹, Yang Li³, Kristen A. Feemster⁴, Scott E. Hensley^{3,#}, David Issadore^{1,5,#}, Arjun Raj^{1,#}

Affiliations

¹ Department of Bioengineering, University of Pennsylvania

² Perelman School of Medicine, University of Pennsylvania

³ Wistar Institute and Department of Microbiology, Perelman School of Medicine, University of Pennsylvania

⁴ Division of Infectious Diseases, Department of Pediatrics, The Children's Hospital of Philadelphia, Perelman School of Medicine, University of Pennsylvania

⁵ Electrical and Systems Engineering, University of Pennsylvania

* Co-first authors

Co-corresponding authors

Abstract

Viral infections are a major cause of human disease, but many require molecular assays for conclusive diagnosis. Current assays typically rely on RT-PCR or ELISA; however, these tests often have limited speed, sensitivity or specificity. Here, we demonstrate that rapid RNA FISH is a viable alternative method that could improve upon these limitations. We describe a platform beginning with software to generate RNA FISH probes both for distinguishing related strains of virus (even those different by a single base) and for capturing large numbers of strains simultaneously. Next, we present a simple fluidic device for reliably performing RNA FISH assays in an automated fashion. Finally, we describe an automated image processing pipeline to robustly identify uninfected and infected samples. Together, our results establish RNA FISH as a methodology with potential for viral point-of-care diagnostics.

Introduction

Viral infections are the cause of a wide range of clinical diseases. While some viral infections can be diagnosed from signs and symptoms alone, for many viral infections, the clinical signs and symptoms overlap with other diseases and infectious agents.¹⁻³ For these reasons, clinicians need laboratory tools to diagnose viral infections. However, currently available viral diagnostics have significant limitations in that they can be very slow, expensive, and are typically not performed at the point-of-care. Overcoming these challenges would enable faster treatment of viral infections, prevent unnecessary doctors office visits, save money, and facilitate large-scale viral surveillance. Here we aim to establish RNA FISH as a methodology for faster, cheaper, and point-of-care viral diagnostic assays.

Most current diagnostic tests target either viral proteins, using immunofluorescence or enzyme-linked immunosorbent assay (ELISA), or viral nucleic acids, using RT-PCR. The vast majority of protein-based diagnostics use antibodies, which require long development times at high costs. In contrast, nucleic acid detection is highly sensitive and highly specific,⁴ and allows easier development of new assays as targets evolve. Detecting nucleic acids by RT-PCR, however, requires 1-2 hours and a thermal cycler, which can be a limitation in common clinical practice,⁵ especially for viruses that are typically treated in a doctor's office or emergency room.

A complementary approach for nucleic acid detection is direct labeling via RNA fluorescence *in situ* hybridization (RNA FISH).^{6,7} Conventionally, RNA FISH has suffered from three main drawbacks preventing its use as a clinical diagnostic: sensitivity, long assay times (6-12 hours), and many complex steps requiring laboratory training.⁶ To overcome sensitivity limitations, we use a variant of RNA FISH developed by Raj et al. that involves hybridization of 20-50 short, fluorescently-labeled oligonucleotide probes to the target RNA.⁸ The use of a large number of oligonucleotides amplifies the fluorescence signal to the point where we can readily detect individual molecules of RNA via conventional fluorescence microscopy. This technique has traditionally required 6-12 hours, but recently our lab has overcome this time requirement by developing a rapid hybridization protocol that utilizes alcohol based fixatives and high concentrations of oligonucleotide probe sets.⁹ Alcohol fixation and permeabilization removes the cell membrane making it possible for oligonucleotides to enter the cell via passive diffusion.

These improvements have reduced the assay time by orders of magnitude such that it can be performed in under five minutes. This rapid assay time indicates great potential for applications in point of care diagnostics, especially for viruses, which generate large numbers of viral RNA. However, open questions remain as to how well RNA FISH can discriminate clinically relevant viruses and whether the assay itself can be standardized and automated to the point where someone without training could run the assay at the point of care.

In this paper, we present a complete platform for viral RNA FISH-based rapid diagnostics that includes viral probe design software, microfluidic automation and image processing software (Fig. 1). First, we created software to design 20 base pair DNA oligonucleotides targeting viral RNA. We formulated two different probing strategies: an algorithm to design probe sets that are capable of targeting many input sequences, and an algorithm to design probe sets that differentiate input sequences from each other. Next, the pipeline includes a microfluidic device to standardize the rapid RNA FISH assay and to make it easily parallelizable for interrogating many viral targets. The microfluidic device concentrates cells under a filter, thereby immobilizing the sample for hybridization of the RNA FISH probes and subsequent washes. Finally, we image the RNA FISH-labeled cells on chip and our image processing software classifies the sample as infected or uninfected.

We selected respiratory viruses as a test bed for developing rapid RNA FISH-based diagnostics because clinicians often treat upper respiratory infections (URI) in outpatient or emergency settings where time is limited and most current tests with rapid turnaround time have significant compromises in analytic sensitivity and/or specificity. As URI symptoms are generally non-specific, molecular diagnostics are especially needed for respiratory viruses because the treatments depend upon what virus (or even bacteria) is causing the symptoms.¹⁰ For example, influenza is effectively treated with neuraminidase inhibitors, oseltamivir and zanamivir, while bacterial infections are treated with antibiotics.^{11,12} In addition to providing relief to the patient with treatment, viral diagnostics help reduce inappropriate use of antibiotics, which is important as it can lead to the development of resistant bacteria. We believe RNA FISH would be particularly useful for respiratory viruses because it could provide the molecular specificity to diagnose these infections.

Results

Probe design algorithms for discriminating viruses

A robust platform needs to address two dichotomous challenges: the need to differentiate between viral strains that have different clinical characteristics but similar sequences, and the need to simultaneously detect viral strains that have highly diverse sequences but similar clinical characteristics. We created probe design software to address both of these possibilities.

To detect different viral strains, we developed a bioinformatic algorithm for designing RNA FISH probes that are specific for each viral strain while exhibiting minimal cross-targeting to other strains. The user provides the total number of DNA oligonucleotides desired in the probe set and the maximum number of bases for which the software will tolerate cross-targeting to

another strain (here, we used 14/20). The software then evaluates every possible 20 base-pair DNA oligonucleotide that can bind to the viral RNA strain of interest. For each oligonucleotide, the software finds the maximum sequence match in the other viral strains, rejecting all oligonucleotides that show a higher degree of sequence complementarity than the user-defined limit. This ensures that none of the oligonucleotides in the strain-specific probe set will cross-hybridize to the other strains (Fig. 2A).

We tested this probe design approach using influenza because multiple influenza strains circulate in the human population at once and discriminating between these strains is clinically useful for treatment and public health purposes. We designed strain-specific influenza RNA FISH probe sets focusing on the strains predicted to be circulating during the 2014-2015 influenza season, specifically A/California/07/2009 H1N1, A/Texas/50/2012 H3N2, and B/Brisbane/60/2008. Influenza is an RNA virus comprised of 8 RNA “segments”, each of which gave high levels of signal by RNA FISH (Supplementary Fig. 1). Further, influenza virus produces both genomic RNA and messenger RNA, each of which also gave high levels of RNA FISH signal with different spatial distributions inside individual cells (Supplementary Fig. 2). We targeted the messenger RNA of the hemagglutinin and nucleoprotein segments with RNA FISH probes for these studies. To test the specificity of our final designs, we infected Madin-Darby canine kidney (MDCK) cells with either H1N1, H3N2, or influenza B. Twenty-four hours after infection, we fixed these cells and performed a five minute hybridization using the RNA FISH probe sets targeting all three viruses. We found that these probe sets specifically bound to cells infected with their corresponding viral strain (Fig. 2B). Furthermore, we found that these strain-specific probes had minimal cross hybridization to the other influenza strains.

Probe design algorithms for targeting many viruses at once

Next, we wanted to develop an assay capable of simultaneously labeling all strains of the same virus despite extensive sequence divergence, which requires targeting each sequence with multiple oligonucleotides. Rhinovirus, for example, has such tremendous sequence diversity that designing a separate pool of 10 oligonucleotides for each of the 348 sequences available on NCBI would require a total of 3480 DNA oligonucleotides, which is prohibitive both in cost and assay complexity. Instead, we sought to create a “pan-probe” set of greatly reduced complexity by targeting oligonucleotides to subsequences that exist in multiple strains. Given a sequence alignment generated by Clustal Omega,¹³ our algorithm seeks to minimize the number of total oligonucleotides in the pool while ensuring that every strain is targeted by at least 10 oligonucleotides. We tested this software on 348 different rhinovirus sequences (including sequences from all three subtypes A, B, and C) available on NCBI, yielding a total of 417 oligonucleotides (Fig. 2D). The maximum number of oligonucleotides targeting any one strain was 31, the minimum was our specified limit of 10, and the mean number of oligonucleotides per strain was 19. The mean number of strains bound by an individual oligonucleotide was 15.7. We also found one oligonucleotide targeting a region in the conserved 5' UTR that binds to 334 of 348 rhinovirus strains.

To test the efficacy of our rhinovirus pan-probe, we infected HeLa cells with one of four different strains of rhinovirus (rhinovirus A1, rhinovirus A16, rhinovirus A81 and rhinovirus B1), fixed them after 24 hours, and performed RNA FISH on each of the four infected samples. With a 5 minute hybridization, we found that the pan-probe was capable of identifying virus in each of the different infections and did not bind to uninfected cells (Fig. 2E). This experiment suggests that we can design a broadly reactive probe set to target all strains of rhinovirus without off-target binding in uninfected cells. We also used this design software to create probe sets for adenovirus viral mRNA and found that these probe sets gave bright fluorescent signal in infected cells (Supplementary Fig. 3).

Design and fabrication of a microfluidic device to concentrate samples, automate rapid RNA FISH, and facilitate imaging

To standardize RNA FISH and facilitate its use, we built a microfluidic device capable of automatically concentrating a dilute sample of cells and performing RNA FISH. The microfluidic chip consists of a track-etched polycarbonate micropore filter positioned between two micromachined sheets of adhesive mylar (Supplementary Fig. 4). Cells in suspension enter the device channel (width 2 mm and length 4 mm) and are concentrated by the filter, which also serves as an imaging area for microscopy (area 7.14 mm²). The filter has a high density of 5 μm (density 10⁶ / cm²), allowing fast flow rates and preventing clogging due to debris. (In particular, if a few of the pores become obstructed, the device continues to operate because fluid can pass through the other pores in the filter.) We anticipate that these features will make the device robust to impurities found in clinical samples such as nasal swabs or sputum¹⁴. The bottom of the chip consists of a microscopy coverslip (number 1 thickness) allowing us to directly image the cells within the device.

To test our device, we performed RNA FISH on influenza infected MDCK cells and imaged the cells using widefield fluorescence and bright-field microscopy and a 20X objective. We scanned the imaging area of the device to obtain a 5 by 8 grid of images, each of which measured 665 μm by 665 μm . This resulted in images at 40 positions that we then assembled into a large panorama covering 3.3 mm by 5.3 mm of the area on the device where the cells are captured on the filter. At each position in the grid, we acquired one bright-field image and three fluorescence images. The fluorescence images were the RNA FISH probe signal, a dapi nuclear stain, and green fluorescent protein (GFP). During analysis, we used the GFP signal to exclude background autofluorescence in the cells. In some assays we included RNA FISH probe sets for more than one virus and obtained additional images with filters that are designed to specifically detect the probe sets (as shown in Fig. 4).

Image processing software and classification of infected and uninfected samples

The next component of our platform is image processing software that aligns and combines the images, finds cells, and classifies them to determine whether samples are positive or negative for virus. Briefly, our image processing module assembles all the individual images into a large panorama and segments the cell nuclei using DAPI, which stains the nucleus (Fig. 3A, steps 1-2). Next, the software calculates the median fluorescence intensity of the RNA FISH signal for each cell (Fig. 3A, step 3). By plotting a histogram of these intensities, we found a peak of

intensity values corresponding to negative cells and a peak corresponding to positive cells (Fig. 3A, step 4). We then used an intensity cutoff to designate, at the single cell level, which cells are positive and which cells are negative and thereby calculate the percentage of infected cells in the sample. Finally, we apply a threshold on the percentage of infected cells in a particular sample to determine whether the overall sample is infected or uninfected. The reason we need this separate threshold is that every sample will have a small number of objects with intensity above the cutoff, but these are essentially always just autofluorescent spots or debris.

We first needed to determine an appropriate intensity cutoff for calling a cell positive and an appropriate threshold of percent cells infected for designating an overall sample as positive or negative. We anticipated that appropriate classification of samples as positive or negative would require simultaneous adjustment of both of these parameters. For instance, if the uninfected cells and infected cells have similar fluorescence intensity, it would be impossible to pick an intensity cutoff that would perfectly designate individual cells as uninfected or infected. In this case, the best intensity cutoff would still designate some uninfected cells as infected, and thus we would need to adjust the percentage infected threshold to avoid designating a negative sample as positive. The percentage of infected cells threshold is also highly dependent upon the total number of infected cells in the sample. For example, if we are assaying a virus that infects every cell in the sample, we would be able to set a high threshold percentage of infected cells to determine whether the overall sample is positive because every positive sample would be above the threshold. By setting a high threshold, we would avoid a situation where a few autofluorescent cells in a negative sample would cause the sample to be incorrectly designated as positive. For these reasons, we performed a series of experiments on our platform using both infected and uninfected samples to establish both assay parameters. We loaded the microfluidic chip with either influenza infected ($n=10$ at 0.26% and $n=9$ at 1.87% infected) or uninfected ($n=11$) MDCK cells and performed RNA FISH for the virus. We imaged the samples on the chip and processed these images with our software to obtain the median fluorescence intensity for each cell.

We used this dataset to determine an appropriate cutoff intensity value for designating an individual cell as infected or uninfected. To find the optimum, we generated receiver-operator characteristic curves for all possible per cell intensity cutoffs by plotting the true positive rate versus the false positive rate at various thresholds for percentage of infected cells. Each receiver-operator curve shows how well the threshold of percentage of cells infected serves to classify samples and is dependent upon the particular intensity cutoff chosen. Thus, we selected the intensity cutoff that produced the best receiver-operator curve for percentage infected and used the area under the receiver-operator curve as the metric for making this decision (Fig. 3A, step 4, optimal cutoff = 330). From here onward, for any cell with median intensity above 330, we classified this cell as positive and for any cell below 330, we classified the cell as negative. Further, to confirm that this experimentally determined intensity value is consistent between infections and experiments, we separately infected another batch of MDCK cells with influenza and performed RNA FISH using the platform. We found that the intensity histogram of the median RNA FISH signal in infected and uninfected cells was similar to our prior infections (Supplementary Fig. 5).

With the cutoff intensity for calling a cell positive established, we next sought to establish a threshold of percentage of infected cells for classifying samples as positive or negative (Fig. 3B). At an input of 1.87% infected cells, we found that choosing a threshold between 0.22% and 0.66% yielded an essentially perfect classifier, with an area under the curve of 1. As we lowered the percentage of infected cells in the input down to 0.26%, the performance of our classifier deteriorated, with an area under the curve of 0.88 and an optimal threshold of 0.21% (Fig. 3B). However, with approximately 1000 cells loaded onto the device for each run, we found that the decline in performance was likely due to randomly sampling only uninfected cells due to the low percentage of infected cells (Supplementary Fig. 6).

With our intensity cutoff established, we wanted to verify that our assay operated consistently. Thus, separate from the data set in Fig. 3B, we performed 10 independent influenza RNA FISH experiments in the device with 1.53% infected cells and determined which cells were positive by applying the RNA FISH intensity cutoff previously established. We again considered the percentage of infected cells as the discrimination variable and plotted a receiver operator characteristic curve by varying this parameter. As before, the curve indicated that we are able to perfectly classify uninfected and infected samples. Taken together, these experiments demonstrate that our viral RNA FISH platform detects influenza and discriminates positive and negative samples with high accuracy and reproducibility.

Multiplex viral detection by integrating specific and pan-probes in the device

One strength of RNA FISH is the ability to multiplex by using multiple probes labeled with differently colored fluorophores on a single sample simultaneously. To demonstrate this ability with our platform, we combined our subtype specific probes and our pan-probes into a single assay that we can run in the device (Fig. 4A). We designed a panel using the subtype specific influenza probe sets (H3N2, H1N1, and influenza B) and rhinovirus pan-probe sets, each labeled with different fluorophores. We then infected MDCK cells with the different influenza strains and infected HeLa cells with rhinovirus. We loaded each of these infected populations into a separate microfluidic device and performed RNA FISH for all four different viruses. For this experiment, we wanted to know if we could identify which virus was causing infection at the single-cell level. By setting the cutoff for calling a cell positive as four standard deviations from the mean intensity of our uninfected control, we were able to clearly identify cells infected with the correct virus (Fig. 4B). We observed minimal off-target labeling, ranging from 0% to 5.8% of cells incorrectly classified as having another virus; however for each virus, the total percentage of miscalled cells was consistently <10% of the total number of cells. Thus, we conclude that this assay is capable of subtyping one virus, pan-probing another virus, all in the device simultaneously on a single sample.

Viral SNP FISH detects drug resistant viruses

In addition to having different subtypes, viruses can also acquire important single base mutations such as those that confer resistance to antiviral medications^{15,16}. However, conventional RNA FISH does not have the specificity to discriminate single bases because a one base mismatch does not create a large difference in relative binding affinity for an entire 20

base oligonucleotide. Our lab has recently developed a modification on RNA FISH that enables us to detect single-nucleotide polymorphisms (SNP) in individual RNA transcripts, and we have demonstrated that it is compatible with rapid hybridization^{9,17}. In order to improve specificity, we use a “mask” oligonucleotide that prevents cross hybridization by magnifying the relative difference in binding energy from a one base mismatch (Fig. 5A). While the mask improves specificity of the assay, any single oligonucleotide will still bind to many off-target sites throughout the cell. Thus, we make a “guide” probe consisting of many fluorescently tagged DNA oligonucleotides that brightly and specifically label individual RNA molecules, thereby showing us where to look for SNP probes that are correctly binding to their target. We then only consider SNP probe signal that co-localizes with the spots from our guide probe.

We tested whether our assay could detect a point mutation in the neuraminidase gene (nucleotide position 823 C → T or amino acid position H274Y in N2 numbering) of influenza A H1N1, which was in circulation prior to 2009^{15,16}. This mutation alters the oseltamivir binding site in neuraminidase making it ineffective in treating influenza (Fig. 5B)¹⁸.

To test whether our assay could reliably distinguish between drug-resistant and wild-type influenza, we infected MDCK cells with wild-type influenza A/California/07/2009 H1N1 and with A/California/07/2009 H1N1 engineered to possess the H274Y (C823T nucleotide) NA mutation. We then used SNP RNA FISH to classify individual transcripts as wild-type or resistant mutant RNA. Qualitatively, we observed that the cells infected with the wild-type virus had RNA classified as predominantly wild-type and vice versa with the mutant (Fig. 5C, Supplementary Fig. 7). For each cell, we compared the relative amounts of each RNA and calculated the ratio of resistant mutant RNA to wild-type RNA (Supplementary Fig. 7). We used this metric as a binary classifier to determine which virus was infecting each cell and created a receiver operator characteristic curve. Each point on the curve represents a potential threshold ratio of resistant mutant RNA to wild-type RNA (Fig. 5D), with points closest to the upper left-hand corner representing thresholds that generated the most sensitive and specific classification. Applying this analysis to our data, we found that a threshold ratio of around 50:50 mutant RNA to wild-type RNA is optimal, which is also intuitively the ideal choice for this threshold. At this 50:50 threshold, the sensitivity of this assay for individual cells is 0.96, and the specificity is 0.97 (false positive rate 0.03).

Discussion

In this paper, we outline a platform for rapid viral detection using RNA FISH, including viral probe design software, a microfluidic device to automate RNA FISH, and image-processing and analysis software to discriminate infected and uninfected samples. To tailor RNA FISH to viruses, we developed probe design software that allows the user to design subtype specific probe sets or probe sets that target many viral strains simultaneously and tested this software using influenza and rhinovirus, respectively. The microfluidic device provides simple, semi-automated, and standardized processing of samples for RNA FISH. Finally, our image-processing software and statistical framework enables automatic classification of infected or uninfected samples. We tested our technology on influenza, rhinovirus, and adenovirus, respiratory viruses that require rapid diagnosis in outpatient and emergency settings. Our

platform demonstrated high classification performance and the ability to target multiple viruses simultaneously. In addition, the entire assay, including the RNA FISH and the imaging, takes only 15 minutes. These components make rapid RNA FISH a viable technology for viral diagnostics.

The distinct advantages of RNA FISH-based viral diagnostics are its speed, cost per test, and flexibility and specificity of the probe design. The two most relevant diagnostic technologies for comparison are RT-PCR and rapid viral antigen tests. RT-PCR is highly sensitive and specific, but requires 1-2 hours to perform in a pathology laboratory¹⁹. In contrast, rapid antigen tests require 5-15 minutes and can be performed at POC¹⁹, but have variable sensitivity and specificity. We believe that RNA FISH combines some advantages of both of these techniques. The overall time to perform RNA FISH on the microfluidic chip is 8 minutes and the imaging typically requires 5 minutes. However, we aim to reduce the device time and imaging time even further as hybridization to influenza RNA can take as little as 30 seconds (Supplementary Fig. 8). Newer influenza diagnostics use isothermal amplification and are significantly faster, between 15-30 minutes^{20,21}. For example, the Alere i Influenza test takes 15 minutes and in the initial clinical studies, performed with a sensitivity 91.8-97.8% and specificity 85.6-96.3%²². This test was CLIA waived in 2014 and may become widely adopted as it offers the speed of rapid antigen tests with sensitivity and specificity approaching that of conventional RT-PCR. However, unlike RNA FISH, this test does not discriminate between viral strains at the single base level, which can be needed to distinguish drug resistant from drug sensitive strains²².

A strength of RT-PCR is its sensitivity, which one study showed was able to detect as little as 10-50 copies of virus per sample²³. While in principle RNA FISH could have sensitivity down to even single molecule resolution, we anticipate that another issue is that if only very few cells are infected, it may lead to false negatives. That said, at low levels of infection, we found that individual cells still produced bright signal, albeit at a reduced frequency (Supplementary Fig 9). If this holds true in clinical samples, it may be possible to improve the sensitivity by imaging many cells. However, there is an upper limit to the total number of cells that will fit into the device without clogging the filter, and we estimate this limit to be around 10,000 cells with our design.

A clear strength of RNA FISH is the flexibility of probe design. The software in our platform makes it easy to generate custom designs to specifically target different viral strains and/or detect many viral strains with one probe set. These features of our software will allow RNA FISH to be performed on emerging viruses and viruses that rapidly mutate, with little development time and cost. While development of probes requires viruses to be sequenced, sequencing is often routine on viruses with a large public health impact and costs are rapidly falling. Combining the probe design and multiplex capabilities as well as the ease of use and low cost of the microfluidic device, RNA FISH could also be used as a surveillance tool to monitor the spread of viral disease. For comparison, antibody-based tests, including rapid antigen tests or ELISAs, use high affinity antibodies, the development of which can take months, requires extensive validation, and is not possible for some targets²⁴. This is a major concern because antibody-based diagnostics may not be readily available during an outbreak of a new virus or if

a virus acquires mutations that prevent binding of the antibody. Similar to RNA FISH, it is possible to quickly develop and deploy new primer sets for conventional RT-PCR assays as was done with the novel H1N1 swine flu in 2009²⁵⁻²⁷. However, this level of flexibility with primer design is not yet possible with the newer and faster isothermal amplification techniques. Thus, currently only RNA FISH combines the ability to quickly design new probe sets with a fast assay turnaround time.

Specificity of the probe sets is another strength of RNA FISH-based viral detection assays. Our data demonstrates that RNA FISH can not only differentiate between strains of virus, but also can detect a single nucleotide mutation in influenza conferring resistance to oseltamivir. Detection of single amino acid changes is often not possible with antibody based diagnostics. While RT-PCR based approaches can detect point mutations, these assays generally have greater complexity, less ease of use, and lower sensitivity than conventional RT-PCR^{28,29}.

While still a nascent technology for clinical use, RNA FISH has the potential to be a very cost effective detection assay. Synthesizing a new RNA FISH probe set for a laboratory scale costs between \$300-\$600 for 10,000 tests, which comes to a total of 3-6 cents per test, and at larger scales, the cost of the probe sets would be even lower. Similarly, we expect the microfluidic device to be inexpensive, particularly at large scales where it could be manufactured with injection molding. While the consumables are cost effective, the equipment needed to image these samples is more expensive. However, many research groups are working on developing low cost and portable microscopes and such equipment would be necessary to use this assay at the point of care³⁰. For comparison, RT-PCR also requires costly equipment including a thermal cycler and uses enzymes which often have limited shelf-life and licensing fees that raise their costs.

In summary, we developed a pipeline for rapid RNA FISH that demonstrated high classification performance, multiplexing ability, and the ability to distinguish individual strains of a virus.. Our work establishes RNA FISH as a viable methodology for rapid detection of viruses with the potential to enable point-of-care diagnostics applications.

Materials and methods

Influenza viruses

We created viruses expressing the A/California/7/2009 HA and NA or A/Puerto Rico/8/1934 HA and NA via reverse genetics as previously described³¹. All of our reverse genetics-based viruses possessed internal A/Puerto Rico/8/1934 genes. We used QuickChange site-directed mutagenesis kits (Stratagene, La Jolla, CA, USA) to introduce the D225G HA mutation into the A/California/7/2009 HA to increase virus yields³². We also used site-directed mutagenesis to introduce the H274Y NA mutation. All reverse genetics-derived viruses were propagated in 10 day old fertilized chicken eggs.

The A/Victoria/361/2011 strain was obtained from Influenza Reagent Resource, Influenza Division, WHO Collaborating Center for Surveillance, Epidemiology and Control of Influenza,

CDC, Atlanta, GA, USA. The B/Florida/4/2006 strain was obtained from BEI Resources, American Type Culture Collection, Manassas, VA, USA. A/Victoria/361/2011 was propagated on Madin-Darby canine kidney cells and B/Florida/4/2006 was propagated in 10 day old fertilized chicken eggs.

For each virus, we used Sanger sequencing to verify that additional mutations did not arise during viral propagation.

Influenza infections

We plated Madin-Darby canine kidney (MDCK) cells on chambered coverglasses (1×10^5 cells/well) or T75 flasks (1.8×10^6 cells/well) 18 hours before infections. Immediately before infection, we washed the cells two times with serum-free media. We then added the viruses to the cell layer at multiplicity of infection of 2-10 in serum-free media with L-(tosylamido-2-phenyl) ethyl chloromethyl ketone (TPCK)-treated trypsin, HEPES, and gentamicin. Twenty four hours after infection, we fixed cells in 100% methanol.

Rhinovirus infections

We purchased the following rhinovirus strains from ATCC: Human rhinovirus 16 (VR-258), Human rhinovirus 1A (VR-1559), Human rhinovirus 81 (VR-1191), and Human rhinovirus 1B (VR-1645).

We grew HeLa cells in T25 flasks to 70% confluency in Dulbecco's modified Eagle's medium with Glutamax (DMEM, Invitrogen) supplemented with 10% fetal bovine serum (FBS), penicillin/streptomycin, 20 mM HEPES, and 40 mM magnesium chloride. We diluted rhinovirus stock at least 1:10 in 2 mL PBS with 0.5% bovine serum albumin. We then washed cells with PBS and added diluted virus. After incubating the cells at 34°C for 1-2 hours, we removed the virus containing medium and added DMEM supplemented with 2% FBS, pen/strep, 20 mM HEPES, and 40 mM MgCl₂. We continued to incubate the cells at 34°C for 16-20 hours, after which we washed the cells in PBS and fixed the cells in ice-cold methanol for 10 minutes.

Adenovirus infections

We grew 293T cells in T25 flasks to 70% confluency in DMEM supplemented with 10% FBS and penicillin/streptomycin (D10F). We washed the cells once with PBS and added 1mL Ad5ΔE1-GFP virus diluted 1:10 in DMEM. We then incubated the cells at 37°C for 1 hour, after which we removed the virus containing medium and added fresh D10F. We continued to incubate the cells at 37°C for 16-20 hours, and then washed the cells in PBS and fixed the cells in ice-cold methanol for 10 minutes.

Device fabrication

We laser cut a piece of clear acrylic for the top layer and two pieces of double sided Mylar tape (thickness = 100 μm, 3M Company) to serve as channel layers (Fig. 1, Supplementary Fig. 4). Between the channel layers, we placed a polycarbonate track-etched film (pore diameter = 5 μm, Whatman, Nuclepore). We assembled the device in a top down fashion by aligning the corners of the acrylic with the laser cut tape and pressing firmly to remove bubbles trapped in

the adhesive layer. We placed the track-etched film on top of the second tape layer and then pressed the first two layers onto the tape, thereby sandwiching the filter. We next attached the bottom layer which is a #1 cover glass (24 mm x 50 mm) to allow for imaging of samples directly on the chip. At the inlet to the device, we secured a laser-cut donut shaped piece of acrylic to create a reservoir for holding liquids. Lastly, we inserted medical tubing into the outlet of the device and secured the tubing with superglue to allow us to pull liquid through the device using a syringe and syringe pump. This allows us to precisely control the flow rate during experimentation. A summary of the syringe pump program for automating flow through the device is included in Supplementary Fig. 10.

Rapid RNA FISH on the microfluidic device

We used a pre-programmed syringe pump to automate the fluid handling in all of the following steps and mounted the microfluidic device onto a 37°C hotplate. For each sample, we fixed the cells in methanol prior to loading on the microfluidic device. After fixation, we loaded 200 µL of the cells in methanol into the fluid reservoir of the device and then pulled the cells onto the device at a flow rate of 100 µL/min. Next, we performed a pre-wash step by loading 200 µL of wash buffer containing 10% formamide and 2X SSC and pulling the solution through the device with the syringe pump. To prepare our hybridization solution, we put 1 µL of each viral RNA FISH probe (at stock concentrations ranging from 1288 ng/µL to 5800 ng/µL) into 500µL of hybridization buffer containing 10% formamide, 2X SSC, and 10% dextran sulfate (w/v). We loaded 80 µL of hybridization solution into the device reservoir and pulled 20 µL onto the sample. We stopped flow through the pump and performed a 5 minute hybridization. At each minute during hybridization, we pulled an additional 4 µL of hybridization solution through the device. After hybridization, we loaded 200 µL of wash buffer into the reservoir and then the pump pulled the buffer through at 200 µL/min. We repeated this wash step 2 additional times for a total of 3 wash steps of 1 minute each. Finally, we applied 200 µL of 2X SSC and imaged the sample. All flow rates were 200 µL/min unless otherwise noted.

Rapid RNA FISH on coverglass

As previously described, we fixed all samples in methanol prior to RNA FISH⁹. We prepared probe solution by combining 50 µL of hybridization buffer containing 10% formamide, 2X SSC, and 10% dextran sulfate with 1 µL of each probe (at stock concentrations ranging from 1288 ng/µL to 5800 ng/µL). For each experiment, we removed all of the methanol from the sample, applied 10 µL of hybridization solution, and covered the sample with a coverslip to disperse the hybridization solution. We hybridized the RNA FISH probes for 5 minutes on a 37°C hotplate. We then washed the samples 3 times for 1 minute at 37°C with wash buffer containing 10% formamide and 2X SSC. Finally, we imaged the cells in 2X SSC.

SNP RNA FISH on coverglass

We adapted SNP RNA FISH protocols previously developed in our lab to target the 823 C -> T mutation in influenza H1N1^{9,17}. Twenty four hours after infection with the virus, we fixed the infected cells using 100% methanol. We prepared a probe solution by combining 50 µL of hybridization buffer containing 10% formamide, 2X SSC, and 10% dextran sulfate with 1 µL of guide probe, 0.5-2 µL of wild-type and mutant probe (volume adjusted to achieve 1:1

concentration ratio of the probes), and mask oligonucleotide at the volume for 2X the concentration of each SNP probe. We removed the methanol from the fixed cells, applied 10 μ L of probe solution, and hybridized the probes for 20 minutes at 37°C on a hotplate. We then washed the sample 3 times for 1 minute at 37°C with wash buffer containing 10% formamide and 2X SSC. Finally, we imaged the cells in 2X SSC.

Microscopy

After RNA FISH, we imaged each samples on a Nikon Ti-E inverted fluorescence microscope using a 20X Nikon Plan objective (numerical aperture 0.40), 100X Plan-Apo objective (numerical aperture of 1.40) and a cooled CCD camera (Andor iKon 934). For 100X imaging, we sequentially acquired three-dimensional stacks of fluorescence images in five different fluorescence channels using filter sets for DAPI, Cy3, Alexa 594, Atto 647N, and Atto 488. Our exposure times ranged from 0.1-2 sec. For SNP FISH specifically, we used exposure times of 3-5 sec. The spacing between consecutive planes in our stacks was 0.3 μ m. For 20X imaging, we scanned the a specified area of interest, and at each position, we acquired one fluorescence image in five different fluorescence channels using filter sets for DAPI, Cy3, Alexa 594, Atto 647N, and Atto 488. The filter sets we used were 31000v2 (Chroma), 41028 (Chroma), SP102v1 (Chroma), a custom set from Omega as described previously ¹⁷, SP104v2 (Chroma) and SP105 (Chroma) for DAPI, Atto 488, Cy3, Alexa 594, Atto 647N and Atto 700, respectively.

Probe design

Pan-probe design software

We implemented our pan-probe design software in MATLAB. The software has 4 main steps: 1) sequence cross-matching, 2) probe elimination, 3) oligonucleotide placement memoization, and 4) oligonucleotide solution readout. In step 1, the software reads an aligned FASTA-format file of sequences and compares 20 base pair oligonucleotides between all sequences for starting at each position in the aligned sequences, yielding cross-matches for all oligonucleotides. In step 2, the software eliminates probes whose hybridization affinities are too far away from a predetermined optimum, determined to be equivalent to around 45% GC ⁸. In step 3, the software uses dynamic programming/memoization to globally optimize the placement of oligonucleotides subject to the goals of minimizing the total number of oligonucleotides while still covering all sequences with a user-defined minimum number of oligos. In step 4, the best solution is read from the memoization table and returned to the user.

Subtype-specific design software

We implemented our subtype-specific probe design software in MATLAB. Our software runs similarly to previous design software ⁸, but in addition to the target sequence, it also accepts a set of other sequences that it tries to avoid. In the context of this manuscript, the target would be the desired viral substrains and the other sequences would be all related substrains that we wish to avoid targeting. Our algorithm screens every candidate oligonucleotide probe (i.e., 20 base oligonucleotides that bind to the target with perfect complementarity) for cross-targeting by excluding all candidates that exhibit more than some user-specified amount of sequence complementarity to all the avoided sequences (in our case, more than 14/20 bases).

Image processing

We implemented our image processing software in MATLAB. First, the software uses phase-correlation to create a montage of individual image tiles. Second, the user defines a region of interest (ROI) to delineate the microscopy viewing area of the device and exclude spurious non-cellular material. The software then stitches together the ROI image for each channel, applying a rolling-ball background subtraction to each included image tile. Third, using the DAPI channel ROI image, nuclei are segmented. The software applies a wavelet filter to filter out high-frequency noise and examine objects about the size of nuclei, thresholds the image using Otsu's method, and then deletes small, edge, and non-circular objects. Each nuclear object is then increased by a 2 pixel radius to create objects that would include both the nucleus and cytoplasm of a typical cell. Fourth, the GFP channel of the image is used as a mask to delete spurious objects that may be the result of dust or other non-cellular objects being trapped by the device filter. The software removes objects that overlap with GFP pixels that are greater than 3 standard deviations above the mean GFP intensity. Fifth, the software determines median viral RNA (vRNA) fluorescence intensity using pixels in each cellular object, a histogram is created, and the fluorescence intensity of the first maxima of the histogram is subtracted from the vRNA fluorescence intensity data to help eliminate device-to-device variability in washes and image acquisition.

SNP FISH image processing

First, we segmented cells and located individual RNA spots using our lab's custom software described in Levesque et al (downloadable at <https://bitbucket.org/arjunrajlaboratory/rajlabimagetools/wiki/Home>). For each spot, we fit a two-dimensional gaussian to determine the location of the spot with sub-pixel resolution. We then performed co-localization by finding the nearest SNP probe signal to every guide spot within a 3.0 pixel range. From this, we obtained the median displacement vector field for each SNP FISH and guide pair and subsequently shifted the image to correct for chromatic deviations. We then repeated the search for colocalization between the guide and SNP probe using a 1.5 pixel range to establish the final colocalization.

Funding

This work was supported by National Institutes of Health [1F30AI114475-01A1 to S.M.S., 1R33EB019767 to A.R., 1DP2OD008514 to A.R., 1R01AI113047 to S.E.H., 1R01AI108686 to S.E.H., T32A1055400 to Y.L., 1R21CA182336-01A1 to D.I.]; and the National Science Foundation [DMR 08-32802 to D.I., 1350601 to A.R.].

Contributions

SMS, RPJ, KAF, SEH, DI, and AR conceived the idea of using rapid RNA FISH as a diagnostic assay for respiratory viruses. SMS, RPJ, DS, AGB, DG, DI, and AR designed and constructed the microfluidic device. SMS, RPJ, BSC, AGB, SEH, DI, and AR designed and performed the RNA FISH experiments for this paper. SMS, RPJ, and AGB analyzed the data for this paper. RPJ and AR wrote the software for viral probe design. RPJ, BSC, YL, and SEH grew the viruses and performed the viral infections. SMS, RPJ, and AR wrote the paper.

Acknowledgements

We thank members of the Raj lab for many helpful discussions. We also thank Biosearch Technologies, specifically Marc Beal and Ron Cook, for reagents and support.

References:

- 1 Y. W. Tang, G. W. Procop and D. H. Persing, *Clin. Chem.*, 1997, **43**, 2021–2038.
- 2 M. Loeffelholz and T. Chonmaitree, *Int J Microbiol*, 2010, **2010**, 126049–5.
- 3 J. B. Mahony, A. Petrich and M. Smieja, *Crit Rev Clin Lab Sci*, 2011, **48**, 217–249.
- 4 S. Yang and R. E. Rothman, *The Lancet Infectious Diseases*, 2004, **4**, 337–348.
- 5 V. Gubala, L. F. Harris, A. J. Ricco, M. X. Tan and D. E. Williams, *Anal. Chem.*, 2012, **84**, 487–515.
- 6 A. Raj and S. Tyagi, *Chapter 17 - Detection of Individual Endogenous RNA Transcripts In Situ Using Multiple Singly Labeled Probes*, Elsevier Inc., 1st edn. 2010, vol. 472.
- 7 Y.-Y. Chou, R. Vafabakhsh, S. Doğanay, Q. Gao, T. Ha and P. Palese, *Proc. Natl. Acad. Sci. U.S.A.*, 2012, **109**, 9101–9106.
- 8 A. Raj, P. van den Bogaard, S. A. Rifkin, A. van Oudenaarden and S. Tyagi, *Nature Methods*, 2008, **5**, 877–879.
- 9 S. M. Shaffer, M.-T. Wu, M. J. Levesque and A. Raj, *PLoS ONE*, 2013, **8**, e75120.
- 10 R. Eccles, *The Lancet Infectious Diseases*, 2005, **5**, 718–725.
- 11 J. Dobson, R. J. Whitley, S. Pocock and A. S. Monto, *Lancet*, 2015, **385**, 1729–1737.
- 12 J. J. Treanor, F. G. Hayden, P. S. Vrooman, R. Barbarash, R. Bettis, D. Riff, S. Singh, N. Kinnersley, P. Ward and R. G. Mills, *JAMA*, 2000, **283**, 1016–1024.
- 13 F. Sievers, A. Wilm, D. Dineen, T. J. Gibson, K. Karplus, W. Li, R. Lopez, H. McWilliam, M. Remmert, J. Söding, J. D. Thompson and D. G. Higgins, *Mol. Syst. Biol.*, 2011, **7**, 539–539.
- 14 M. Muluneh, W. Shang and D. Issadore, *Adv Healthc Mater*, 2014, **3**, 1078–1085.
- 15 N. J. Dharan, L. V. Gubareva, J. J. Meyer, M. Okomo-Adhiambo, R. C. McClinton, S. A. Marshall, K. St George, S. Epperson, L. Brammer, A. I. Klimov, J. S. Bresee, A. M. FryOseltamivir-Resistance Working Group, *JAMA*, 2009, **301**, 1034–1041.
- 16 J. D. Bloom, L. I. Gong and D. Baltimore, *Science*, 2010, **328**, 1272–1275.
- 17 M. J. Levesque, P. Ginart, Y. Wei and A. Raj, *Nature Methods*, 2013, **10**, 865–867.
- 18 K. Das, J. M. Aramini, L.-C. Ma, R. M. Krug and E. Arnold, *Nat. Struct. Mol. Biol.*, 2010, **17**, 530–538.
- 19 S. Kumar and K. J. Henrickson, *Clin. Microbiol. Rev.*, 2012, **25**, 344–361.
- 20 P. Craw and W. Balachandran, *Lab Chip*, 2012, **12**, 2469–2486.
- 21 S. Nie, R. B. Roth, J. Stiles, A. Mikhlina, X. Lu, Y.-W. Tang and N. E. Babady, *Journal of Clinical Microbiology*, 2014, **52**, 3339–3344.
- 22 J. Bell, A. Bonner, D. M. Cohen, R. Birkhahn, R. Yogev, W. Triner, J. Cohen, E. Palavecino and R. Selvarangan, *J. Clin. Virol.*, 2014, **61**, 81–86.
- 23 G. Boivin, S. Côté, P. Déry, G. De Serres and M. G. Bergeron, *Journal of Clinical Microbiology*, 2004, **42**, 45–51.
- 24 J. Bordeaux, A. Welsh, S. Agarwal, E. Killiam, M. Baquero, J. Hanna, V. Anagnostou and D. Rimm, *BioTechniques*, 2010, **48**, 197–209.
- 25 D. M. Whiley, S. Bialasiewicz, C. Bletchly, C. E. Faux, B. Harrower, A. R. Gould, S. B. Lambert, G. R. Nimmo, M. D. Nissen and T. P. Sloots, *J. Clin. Virol.*, 2009, **45**, 203–204.
- 26 R. Wang, Z.-M. Sheng and J. K. Taubenberger, *Journal of Clinical Microbiology*, 2009, **47**, 2675–2677.
- 27 L. L. M. Poon, K. H. Chan, G. J. Smith, C. S. W. Leung, Y. Guan, K. Y. Yuen and J. S. M. Peiris, *Clin. Chem.*, 2009, **55**, 1555–1558.

- 28 W. Wang, Z. Song, W. Guan, Y. Liu, X. Zhang, L. Xu, J. Li, Z. Yuan and Y. Hu, *Emerging Infect. Dis.*, 2014, **20**, 847–849.
- 29 D. J. Operario, M. J. Moser and K. St George, *Journal of Clinical Microbiology*, 2010, **48**, 3517–3524.
- 30 D. N. Breslauer, R. N. Maamari, N. A. Switz, W. A. Lam and D. A. Fletcher, *PLoS ONE*, 2009, **4**, e6320.
- 31 L. Martínez-Sobrido and A. García-Sastre, *J Vis Exp*, 2010, e2057–e2057.
- 32 S. L. Linderman, B. S. Chambers, S. J. Zost, K. Parkhouse, Y. Li, C. Herrmann, A. H. Ellebedy, D. M. Carter, S. F. Andrews, N.-Y. Zheng, M. Huang, Y. Huang, D. Strauss, B. H. Shaz, R. L. Hodinka, G. Reyes-Terán, T. M. Ross, P. C. Wilson, R. Ahmed, J. D. Bloom and S. E. Hensley, *Proc. Natl. Acad. Sci. U.S.A.*, 2014, **111**, 15798–15803.

Figure legends:

Fig. 1: RNA FISH platform rapidly determines whether samples are uninfected or infected with a virus. The pipeline includes probe design software to generate subtype specific probe sets or probe sets that label many viral subtypes. Next, we perform RNA FISH on the microfluidic chip which consists of a 5 minute hybridization and 3 one minute wash steps. Finally, we image the sample directly on the chip and then our image processing pipeline determines whether a sample is uninfected or infected.

Fig. 2: Subtype-specific RNA FISH probes discriminate influenza subtypes and rhinovirus “pan-probe” targets all rhinovirus strains. A) Overview of our subtype-specific probing strategy, in which we design oligonucleotides that only bind to one influenza subtype and do not cross hybridize to other subtypes. B) We used this software to design probes to target A/California/07/2009 H1N1, A/Texas/50/2012 H3N2, and B/Brisbane/60/2008. We then infected MDCK cells with A/California/07/2009, A/Victoria/361/2011, and B/Florida/4/2006 and performed RNA FISH with subtype-specific probes. These three strains of influenza that were close enough in sequence similarity to our designs that we would expect our subtype-specific probes to bind. The RNA FISH probes produce bright fluorescent signal in the subtype to which they are designed and do not produce signal in the other subtypes. DAPI stain labels nuclei in blue, and RNA FISH is in white. C) Overview of “pan-probe” design, in which we optimize for the minimum number of oligonucleotides that will bind to all sequences. D) We used our “pan-probe” software to design RNA FISH probes that target 348 rhinovirus sequences with a minimum of 10 oligonucleotides per strain. The results of this design are summarized by the heatmap where each box represents a pair between an RNA FISH oligonucleotide and a viral strain. Light blue boxes indicate that the oligonucleotide is a perfect match somewhere in the virus and thus should bind, while dark blue boxes represent that the oligonucleotide does not bind to that strain. E) We infected HeLa cells with different strains of rhinovirus and performed rapid RNA FISH with the “pan-probe” for rhinovirus. Cells infected with each strain had bright fluorescent signal by RNA FISH and the uninfected cells remained dark. DAPI (nuclear stain) is in blue, and RNA FISH is in white. White scale bar represents 5 μm .

Fig. 3: Automated computational analysis demonstrates high specificity and sensitivity for viral detection. A) Overview of our image analysis software, in which microscopy images are

automatically stitched, viral RNA (vRNA) fluorescence intensity is measured in and surrounding each DAPI-stained nucleus, and the percentage of positive cells is calculated using a cutoff that best distinguishes devices with infected cells from uninfected cells. B) Histogram and receiver operating characteristic curves for devices with 1.87% and 0.26% percent infected samples. C) Optimized intensity cutoff from A and applied to an independent dataset of uninfected devices and devices with 1.53% infected samples. White scale bar represents 25 microns.

Fig. 4: Multiplex RNA FISH detects four different viruses in one test. (A) We used an RNA FISH probe cocktail including probe sets for influenza A H1N1, influenza A H3N2, influenza B, and rhinovirus labeled with four different fluorophores. For each virus, we loaded the chip with infected cells and hybridized on the probe cocktail. (B) We found that the probe sets brightly labeled the correct virus with minimal fluorescence from the probe sets for other viruses. In the analysis, we set the cutoff for calling a cell positive as four standard deviations from the mean intensity of the uninfected control. The numbers in the upper right-hand corner of each image indicate the percentage of cells designated as positive for that virus. DAPI (nuclear stain) is in blue, and RNA FISH is in white. All images are 20X magnification. White scale bar represents 25 μm .

Fig. 5: Viral SNP FISH detects drug resistant viruses with one base pair sequence difference. (A) We use a “mask” oligonucleotide to improve the specificity of a single probe by magnifying the relative energy contribution from a one base mismatch. (B) We use the SNP FISH technique to detect a point mutation in the neuraminidase gene that changes a histidine to a tyrosine, which alters the structure of neuraminidase such that the neuraminidase inhibitor oseltamivir is less effective in treating influenza. (C) Here, we infected MDCK cells with wild-type influenza A H1N1 and mutant influenza A H1N1 containing the oseltamivir resistance mutation. Representative images of SNP FISH on these cells show that most RNA transcripts are correctly labeled by the probes. DAPI (nuclear stain) is in blue, and RNA FISH is in white. Both images are 100X magnification. White scale bar represents 5 μm . (D) A receiver-operator characteristic curve demonstrates that this assay is effective for classifying cells as infected with wild-type or resistant mutant virus.

Figure 1

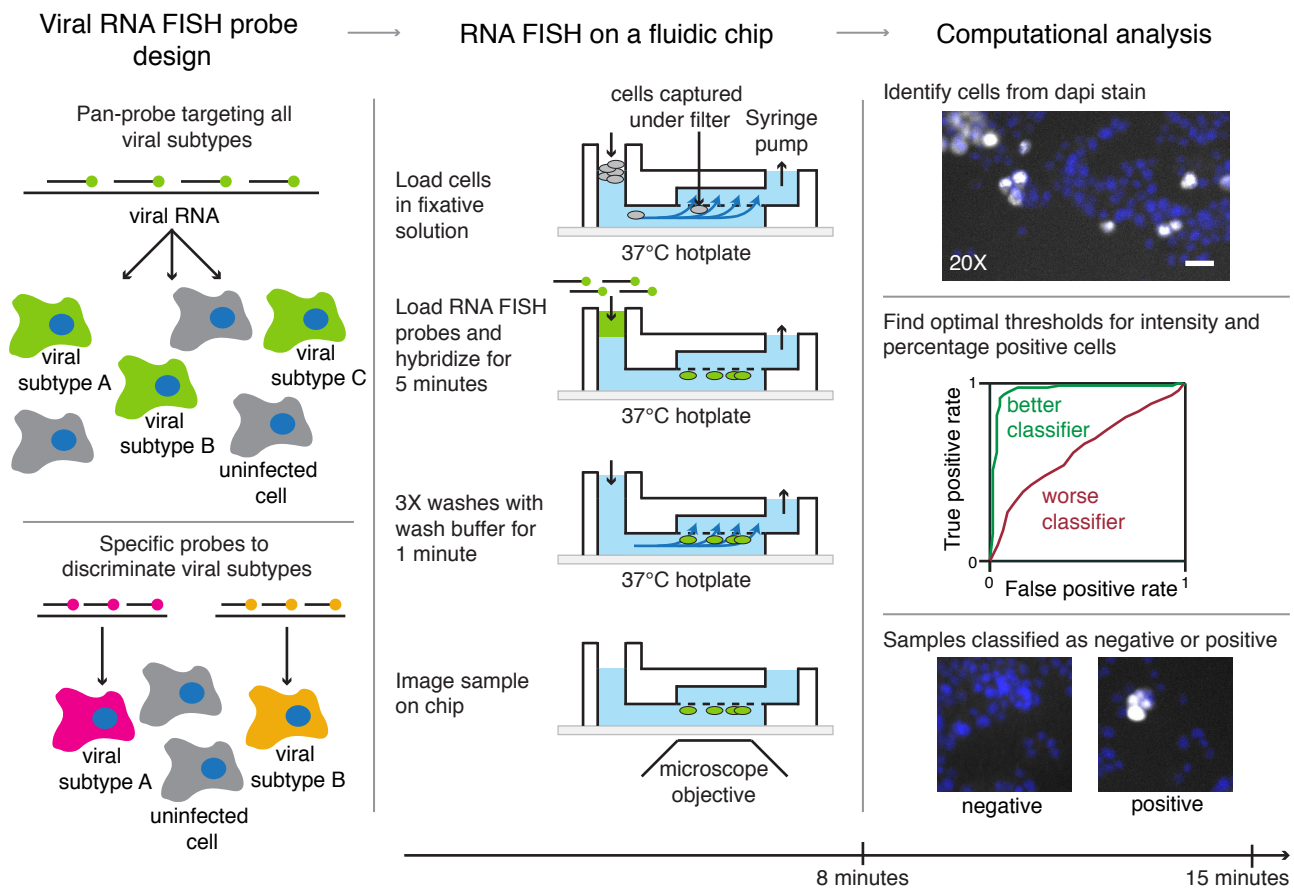


Figure 2

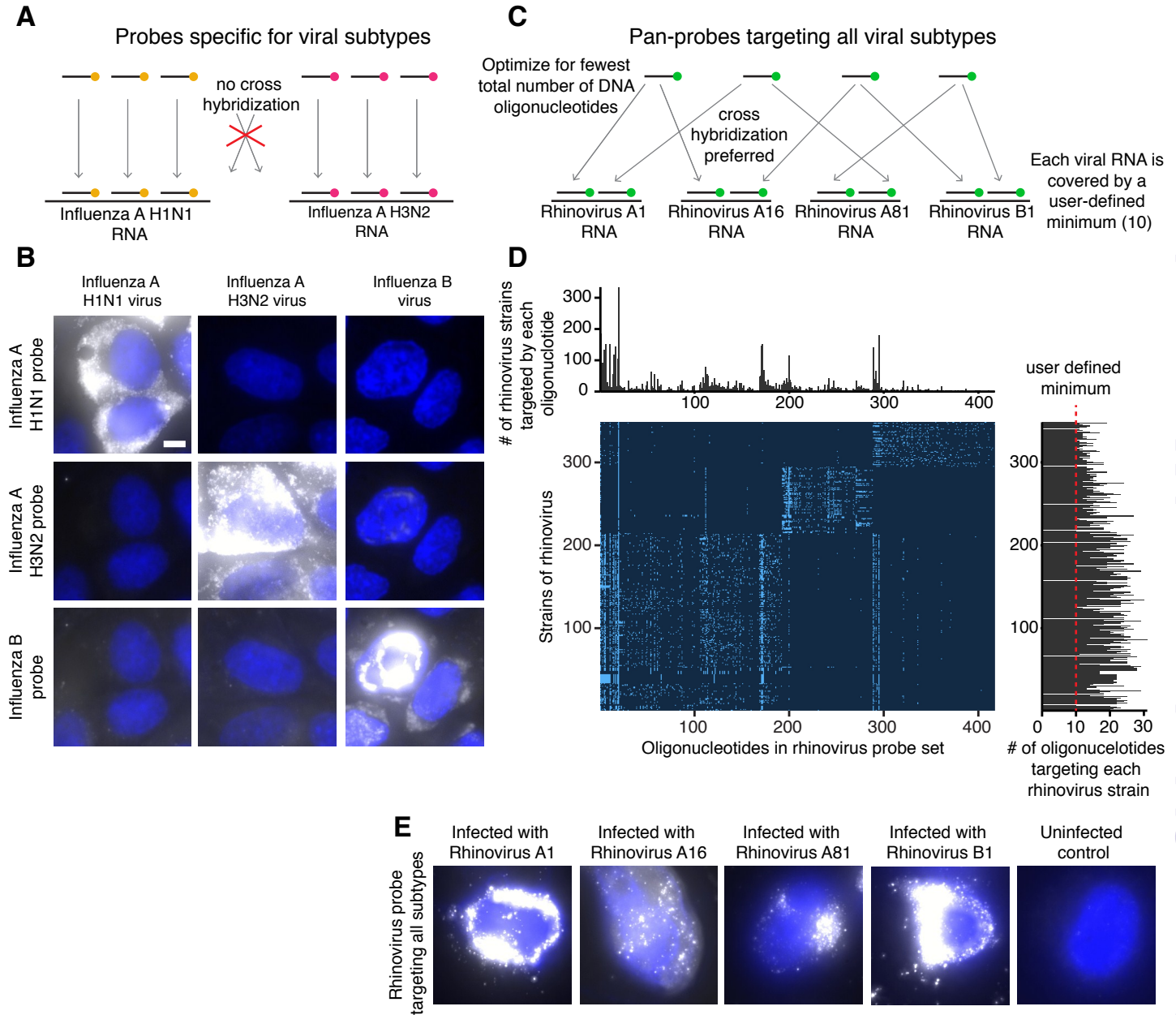


Figure 3

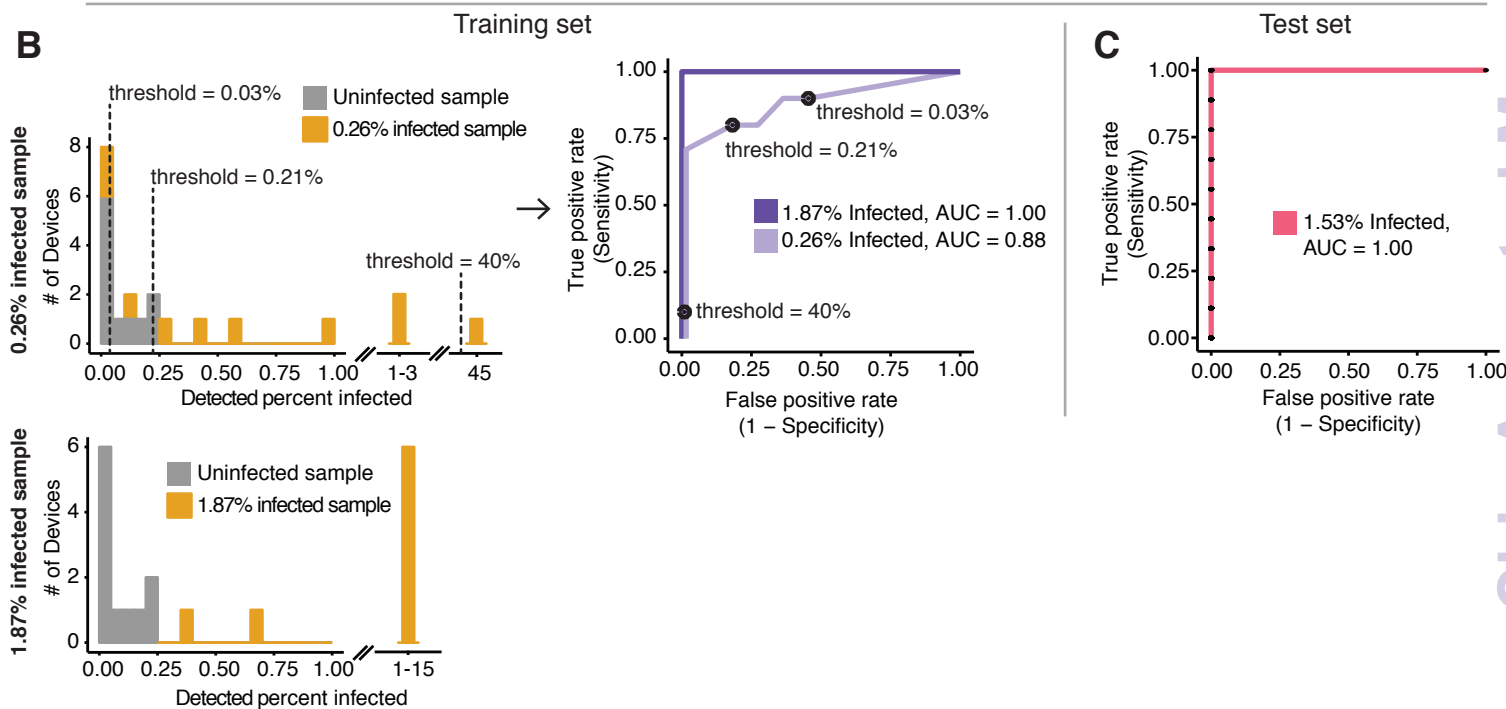
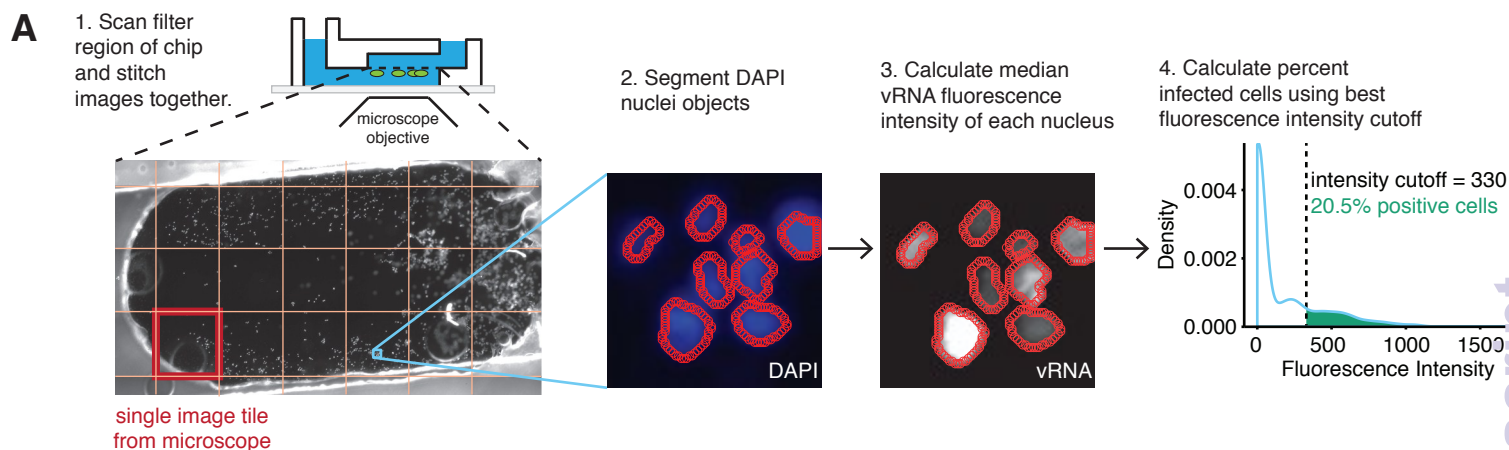


Figure 4

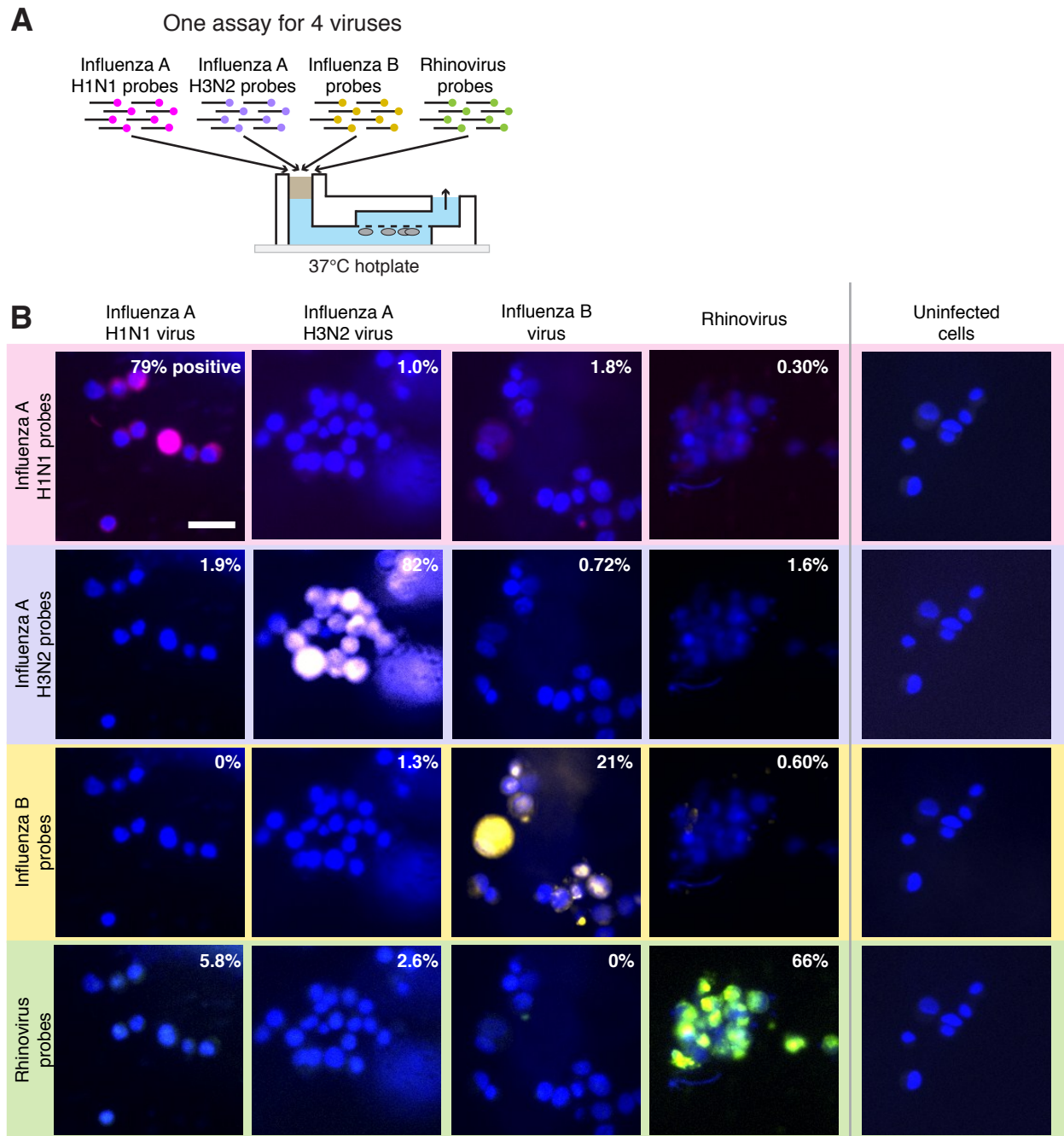
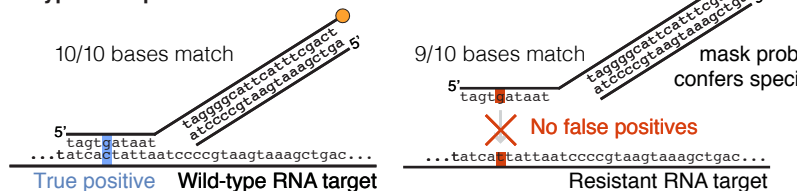


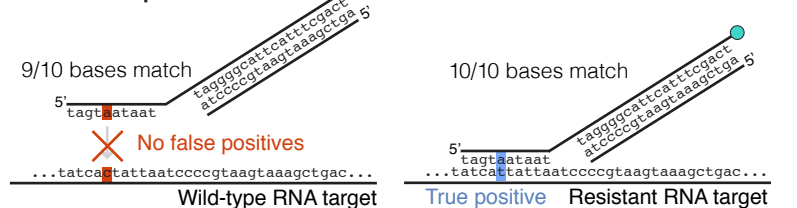
Figure 5

A Single-base discrimination with SNP FISH

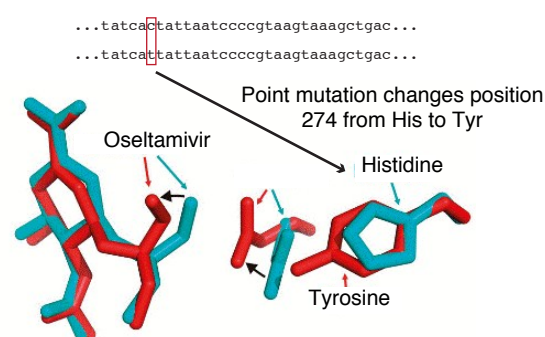
Wild-type virus probe



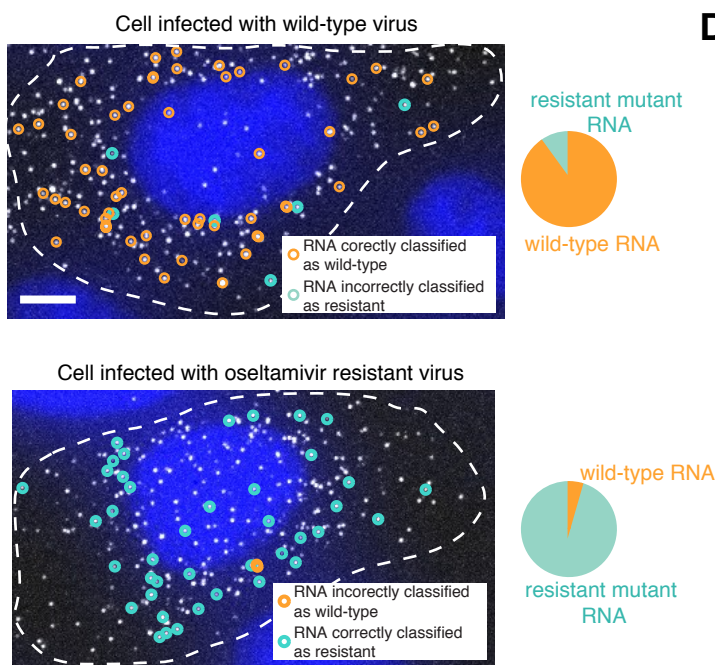
Resistant virus probe



B



C



D

Receiver operator characteristic for classification using the ratio of mutant to wild-type RNA

